SUPPORTING INFORMATION

Halide Effects on the Stability of Osmium Indenylidene Complexes: Isolation, Characterization and Reactivities

Mingxu Cui, Xueying Guo, Herman H. Y. Sung, Ian D. Williams,* Zhenyang Lin,* and Guochen Jia*

Department of Chemistry, The Hong Kong University of Science and Technology, Clear Water Bay, Kowloon, Hong Kong, China

Email: chjiag@ust.hk.

Content

1. X-ray Crystallographic Study of **6I** and **8Cl(BPh$_4$)**. S2

2. NMR Spectra S6

1. X-ray Crystallographic Study of 6I and 8Cl(BPh_4).

Table S1. Crystal data of **6I**

	Complex **6I**
Empirical formula	$C_{23}H_{28}I_2Os$
Formula weight	748.45
Temperature/K	100.01(10)
Crystal system	monoclinic
Space group	$P2_1/c$
a/Å	12.2006(2)
b/Å	10.46920(19)
c/Å	17.2843(3)
α/°	90
β/°	94.5738(15)
γ/°	90
Volume/Å^3	2200.70(7)
Z	4
ρ_{calc}g/cm^3	2.259
μ/mm^{-1}	32.987
F(000)	1392.0
Crystal size/mm^3	0.08 × 0.06 × 0.03
Radiation	CuKα (λ = 1.54184)
2Θ range for data collection/°	7.268 to 134.984
Index ranges	$-14 \leq h \leq 13$, $-6 \leq k \leq 12$, $-20 \leq l \leq 20$
Reflections collected	6832
Independent reflections	3926 [R_{int} = 0.0290, R_{sigma} = 0.0413]
Data/restraints/parameters	3926/42/241
Completeness to theta = 66.5°	98.9%
Goodness-of-fit on F^2	1.004
Final R indexes [I>=2σ (I)]	R_1 = 0.0240, wR_2 = 0.0536
Final R indexes [all data]	R_1 = 0.0269, wR_2 = 0.0550
Largest diff. peak/hole / e Å^{-3}	1.04/-1.26

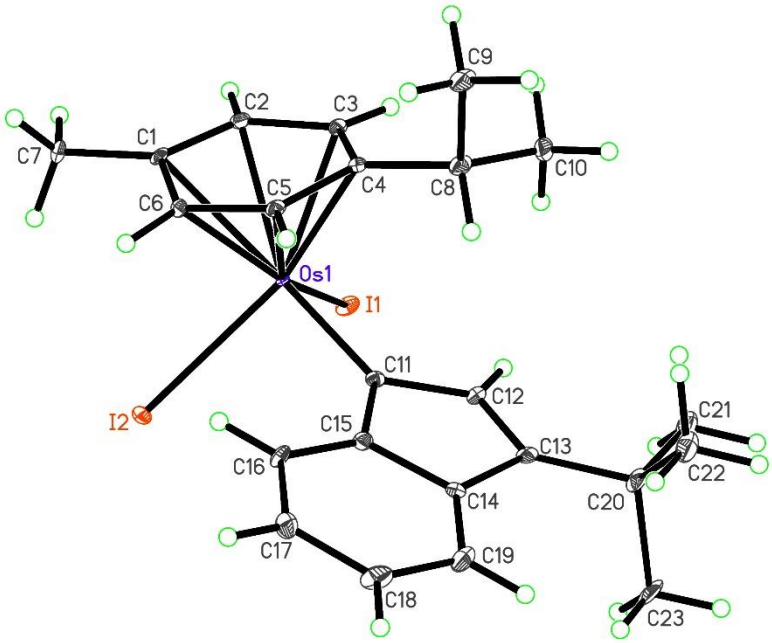

Figure S1. The molecular structure of **6I**. Selected bond distances (Å) and angles (deg.): Os(1)-I(1) 2.7399(3), Os(1)-I(2) 2.7092(3), Os(1)-C(1) 2.384(4), Os(1)-C(2) 2.318(4), Os(1)-C(3) 2.217(5), Os(1)-C(4) 2.248(5), Os(1)-C(5) 2.191(4), Os(1)-C(6) 2.204(4), Os(1)-C(11) 1.949(4), C(11)-C(12) 1.453(6), C(12)-C(13) 1.349(7), C(11)-C(15) 1.477(6), C(14)-C(15) 1.421(7), C(13)-C(14) 1.501(6), I(1)-Os(1)-I(2) 89.439(10), I(1)-Os(1)-C(11) 90.91(12), I(2)-Os(1)-C(11) 92.85(14).

Table S2. Crystal data of **8Cl(BPh$_4$)**

	Complex **8Cl(BPh$_4$)**
Empirical formula	$C_{47}H_{48}BClOs$
Formula weight	849.31
Temperature/K	100.01(10)
Crystal system	monoclinic
Space group	Cc
a/Å	21.1328(2)
b/Å	9.70292(8)
c/Å	20.0078(2)
α/°	90
β/°	114.8617(14)
γ/°	90
Volume/Å^3	3722.38(8)
Z	4
ρ_{calc}g/cm^3	1.515
μ/mm^{-1}	7.365
F(000)	1712.0
Crystal size/mm^3	0.08 × 0.06 × 0.05
Radiation	CuKα (λ = 1.54184)
2Θ range for data collection/°	9.224 to 134.98
Index ranges	$-22 \leq h \leq 25$, $-10 \leq k \leq 11$, $-23 \leq l \leq 19$
Reflections collected	10028
Independent reflections	5212 [R_{int} = 0.0183, R_{sigma} = 0.0240]
Data/restraints/parameters	5212/2/457
Completeness to theta = 66.5°	99.9%
Goodness-of-fit on F^2	1.010
Final R indexes [I>=2σ (I)]	R_1 = 0.0146, wR_2 = 0.0354
Final R indexes [all data]	R_1 = 0.0150, wR_2 = 0.0356
Largest diff. peak/hole / e Å^{-3}	0.56/-0.40
Flack parameter	-0.028(5)

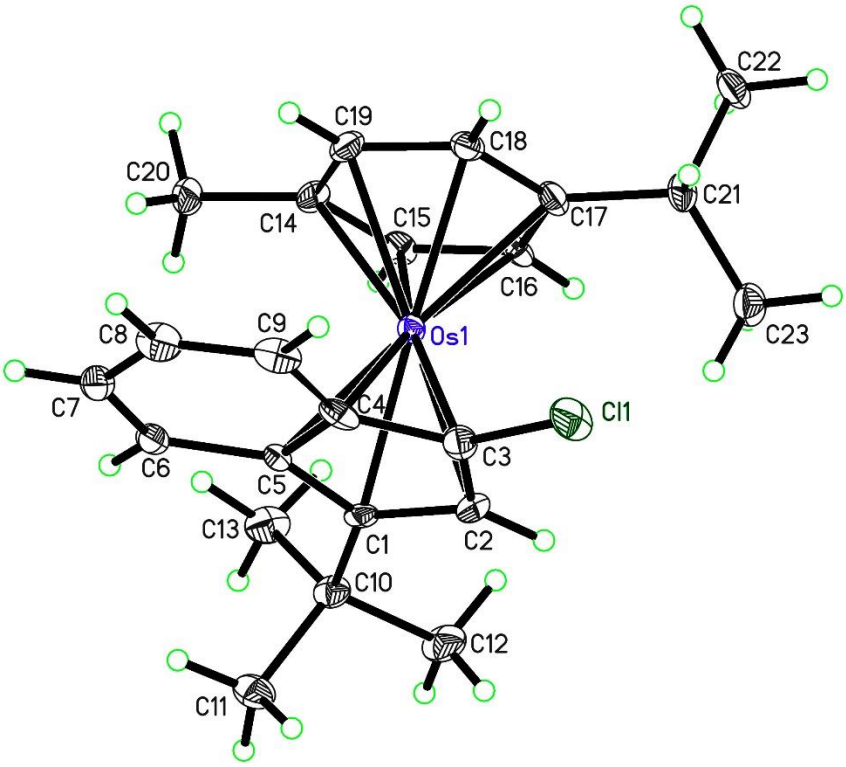

Figure S2. The molecular structure of **8Cl(BPh$_4$).** The counter anion BPh$_4^-$ is omitted for clarity. Selected bond distances (Å) and angles (deg.): Os(1)-C(1) 2.212(3), Os(1)C(2) 2.202(5), Os(1)-C(3) 2.178(6), Os(1)-C(4) 2.247(4), Os(1)-C(5) 2.222(5), Os(1)-C(14) 2.235(4), Os(1)-C(15) 2.219(3), Os(1)-C(16) 2.207(4), Os(1)-C(17) 2.237(6), Os(1)-C(18) 2.219(4), Os(1)-C(19) 2.203(6), Cl(1)-C(3) 1.723(7).

2. NMR Spectra

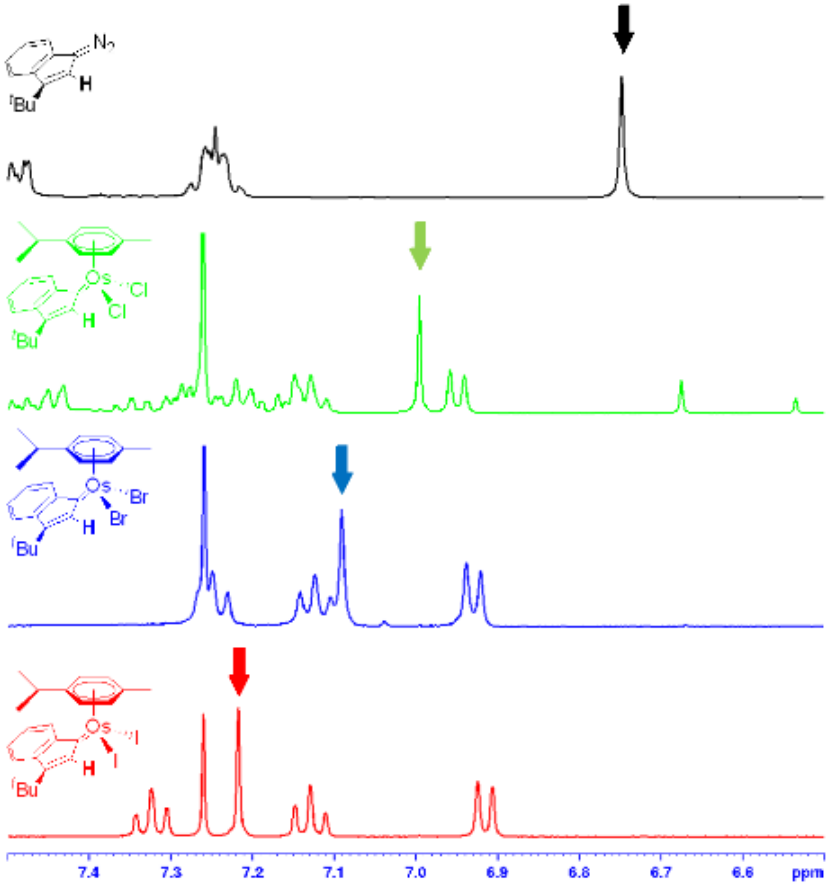

Figure S3. Comparison of the ^{1}H NMR spectra of **1** with those of **6Cl**, **6Br** and **6I**. The spectrum of **6Cl** is an in-situ spectrum. The indenyl β-H signals are marked with arrows.

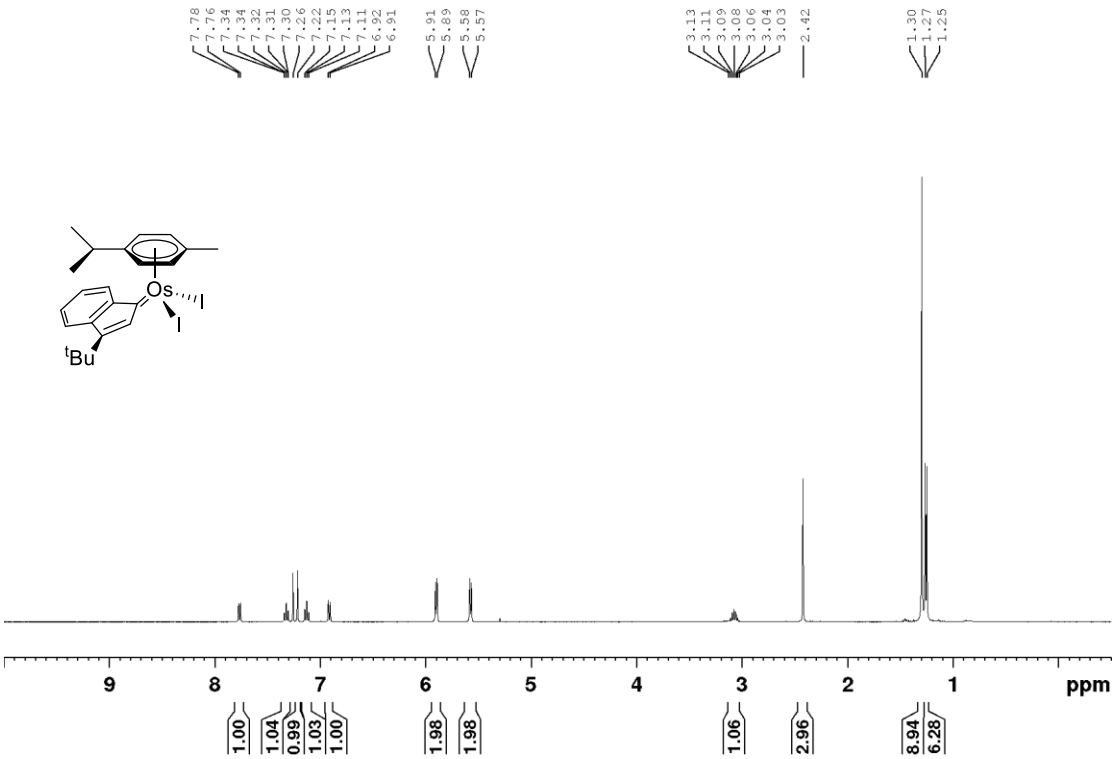

Figure S4. The ^{1}H NMR spectrum of (η^{6}-*p*-cymene)OsI_2[=C_9H_5(^{t}Bu)] (**6I**) in $CDCl_3$ at 400.1 MHz.

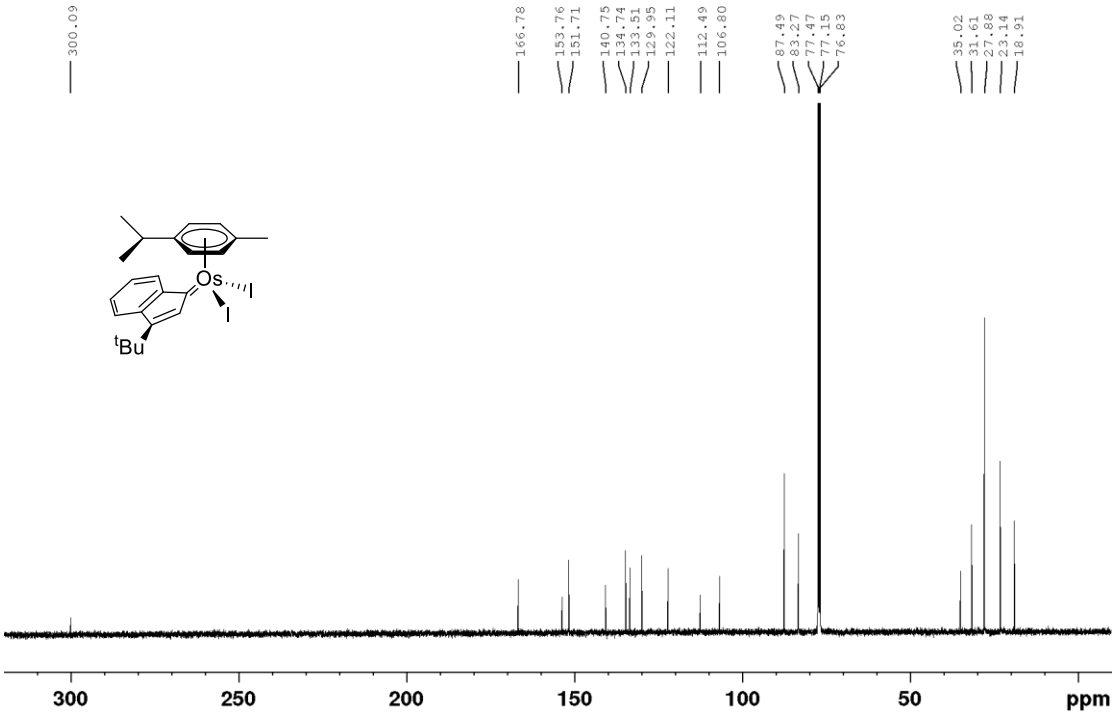

Figure S5. The ^{13}C{^{1}H} NMR spectrum of (η^{6}-*p*-cymene)OsI_2[=C_9H_5(^{t}Bu)] (**6I**) in $CDCl_3$ at 100.6 MHz.

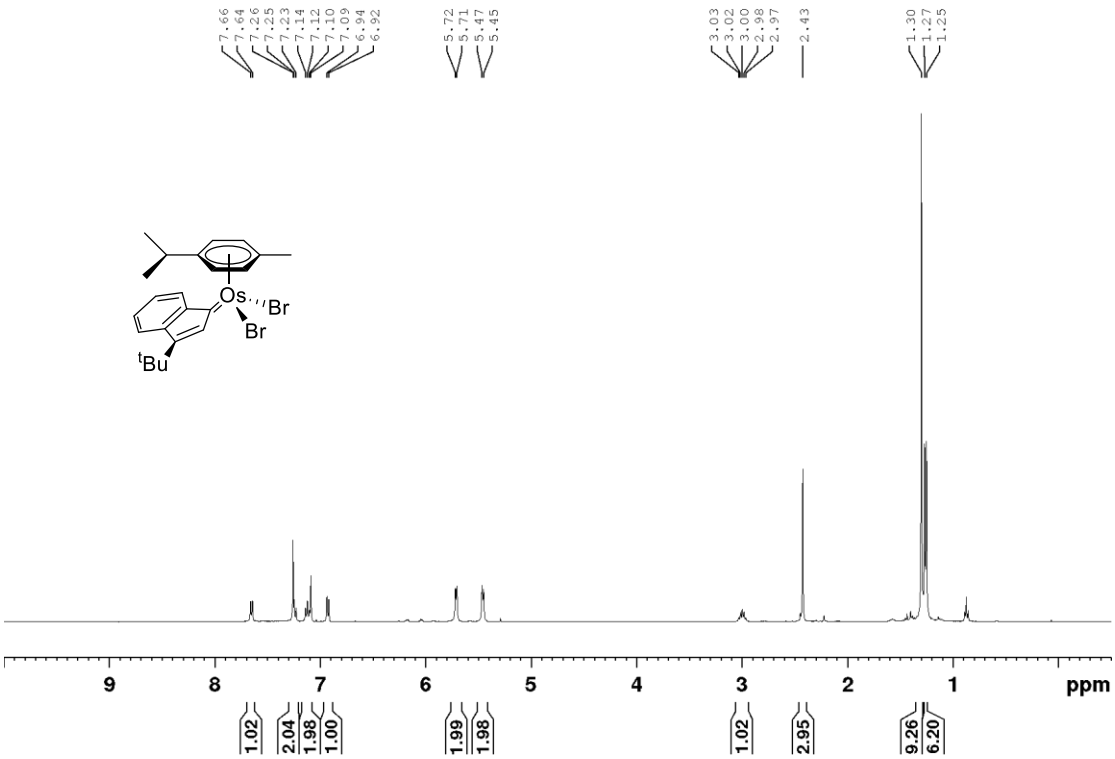

Figure S6. The ^{1}H NMR spectrum of (η^6-*p*-cymene)$OsBr_2$[=C_9H_5(^{t}Bu)] (**6Br**) in $CDCl_3$ at 400.1 MHz.

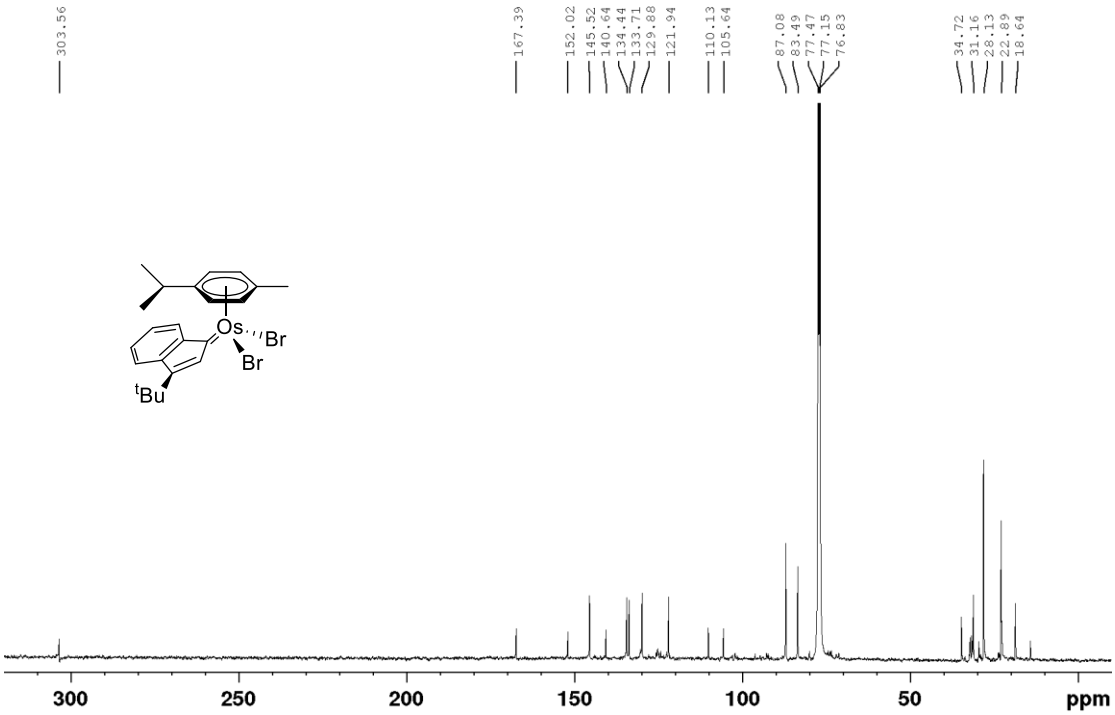

Figure S7. The ^{13}C{^{1}H} NMR spectrum of (η^6-*p*-cymene)$OsBr_2$[=C_9H_5(^{t}Bu)] (**6Br**) in $CDCl_3$ at 100.6 MHz.

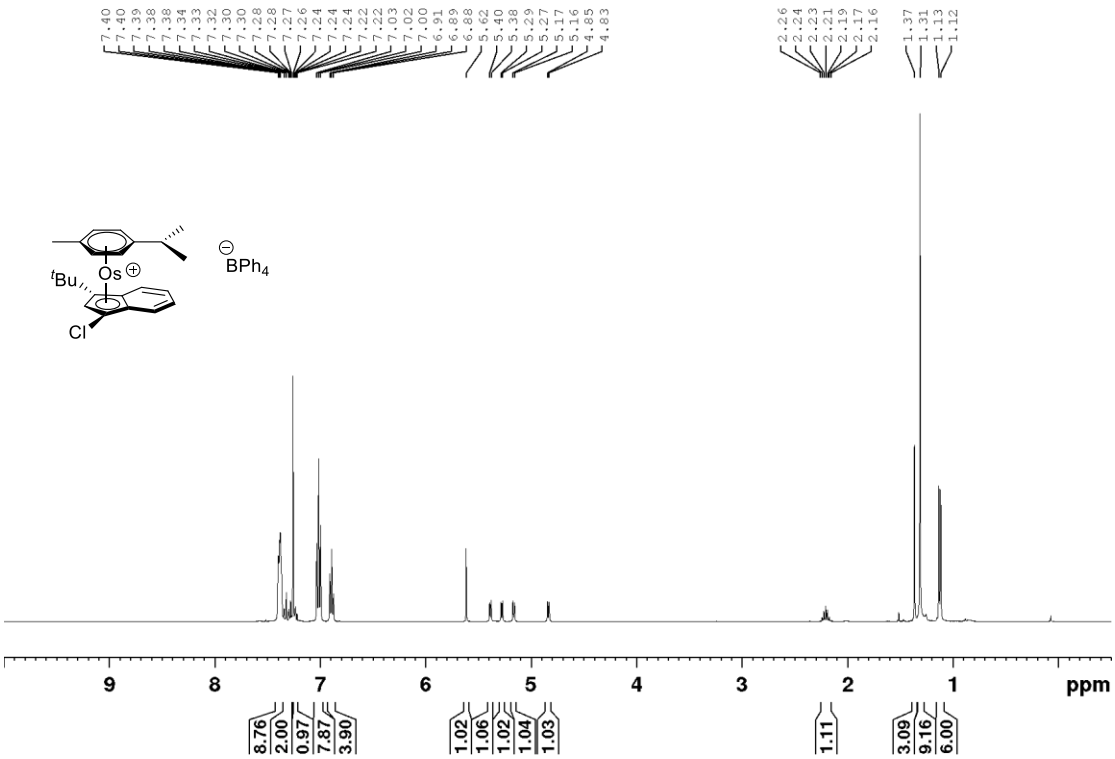

Figure S8. The ^{1}H NMR spectrum of {(η^6-*p*-cymene)Os[η^5-C_9H_5(^{t}Bu)Cl]}BPh_4 [**8Cl(BPh$_4$)**] in $CDCl_3$ at 400.1 MHz.

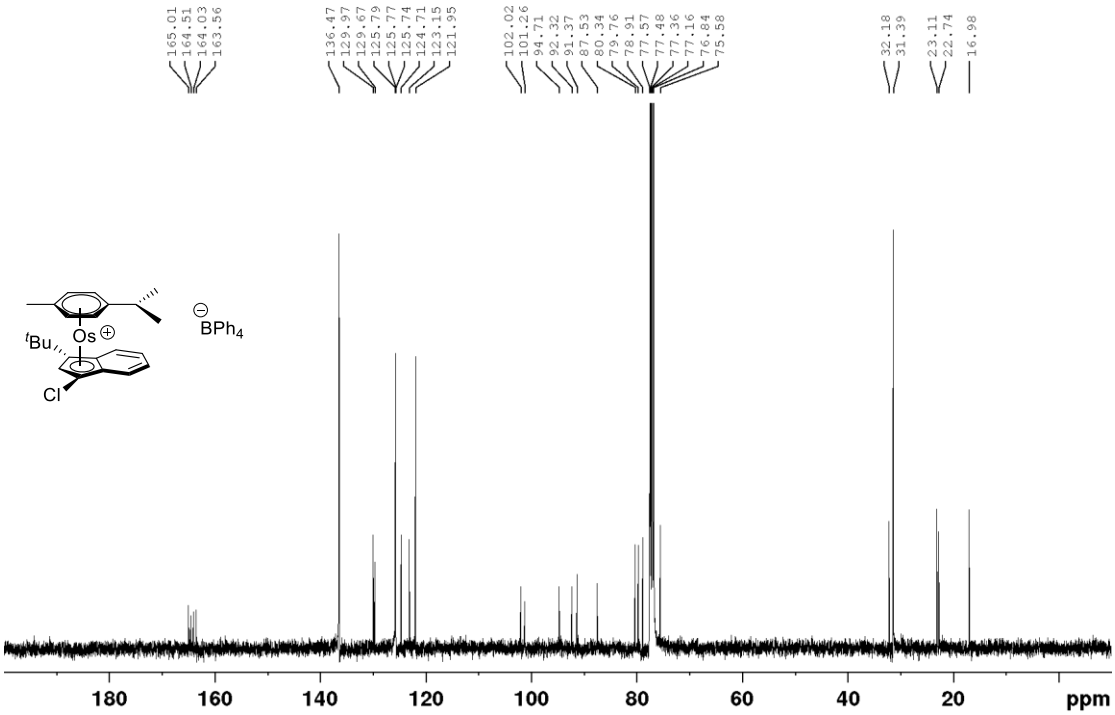

Figure S9. The ^{13}C{^{1}H} NMR spectrum of {(η^6-*p*-cymene)Os[η^5-C_9H_5(^{t}Bu)Cl]}BPh_4 [**8Cl(BPh$_4$)**] in $CDCl_3$ at 100.6 MHz.

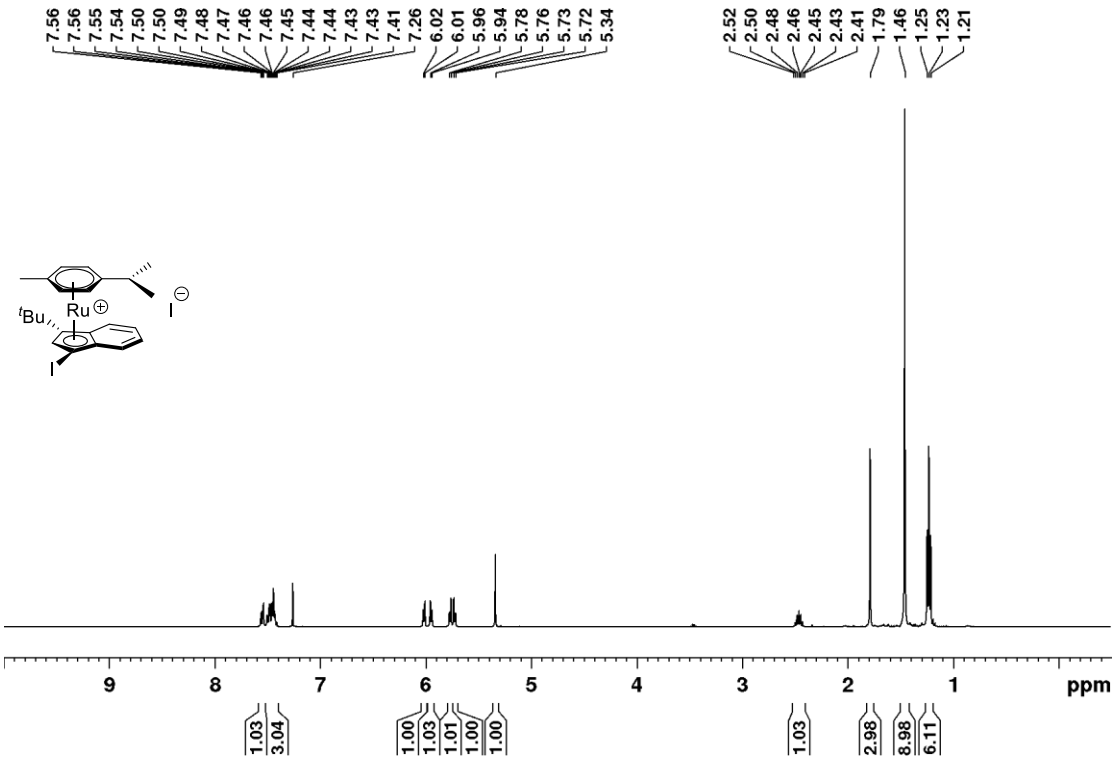

Figure S10. The ^{1}H NMR spectrum of {(η^{6}-*p*-cymene)Ru[η^{5}-C_9H_5(^{t}Bu)I]}I (**9**) in $CDCl_3$ at 400.1 MHz.

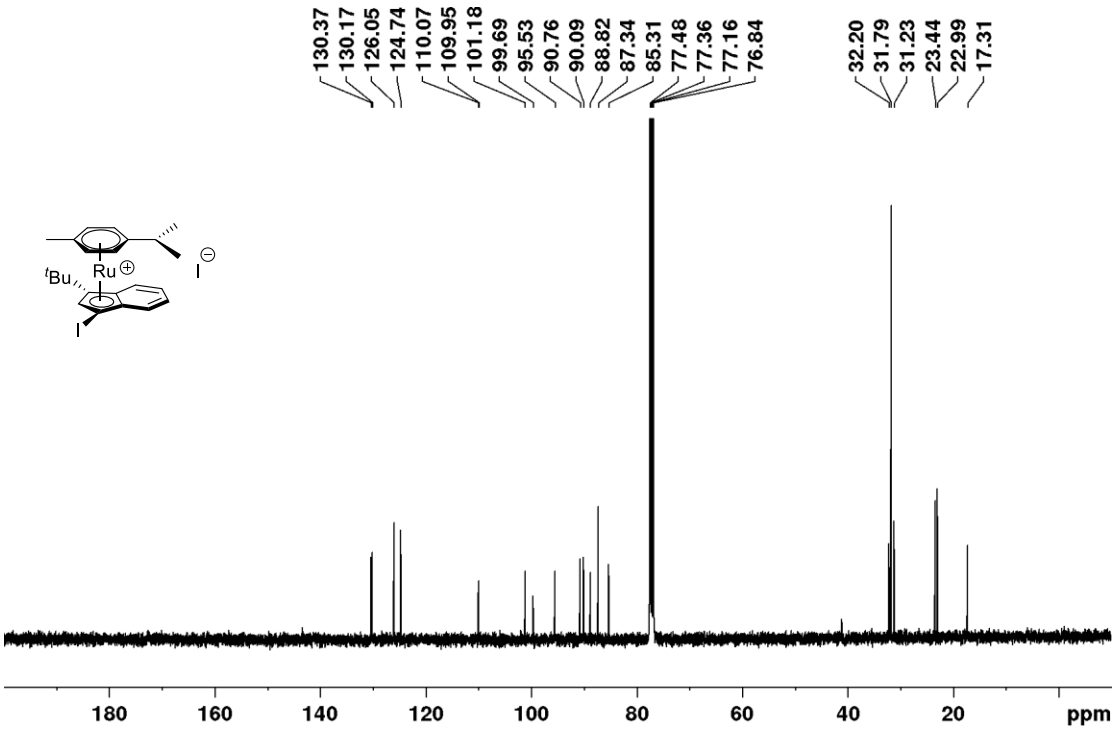

Figure S11. The ^{13}C{^{1}H} NMR spectrum of {(η^{6}-*p*-cymene)Ru[η^{5}-C_9H_5(^{t}Bu)I]}I (**9**) in $CDCl_3$ at 100.6 MHz.

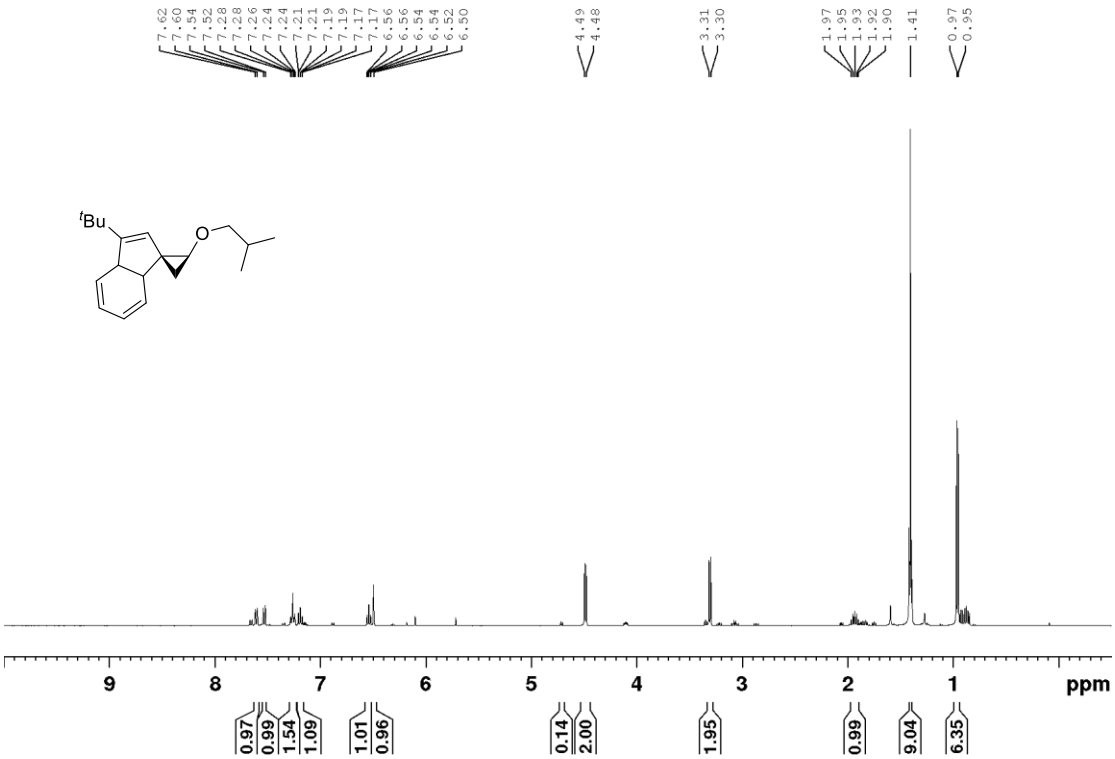

Figure S12. The ^{1}H NMR spectrum of 2-*iso*-butyloxy-2'-*tert*-butylspiro[cyclopropane-1,1-indene] (**3a**) in $CDCl_3$ at 400.1 MHz.

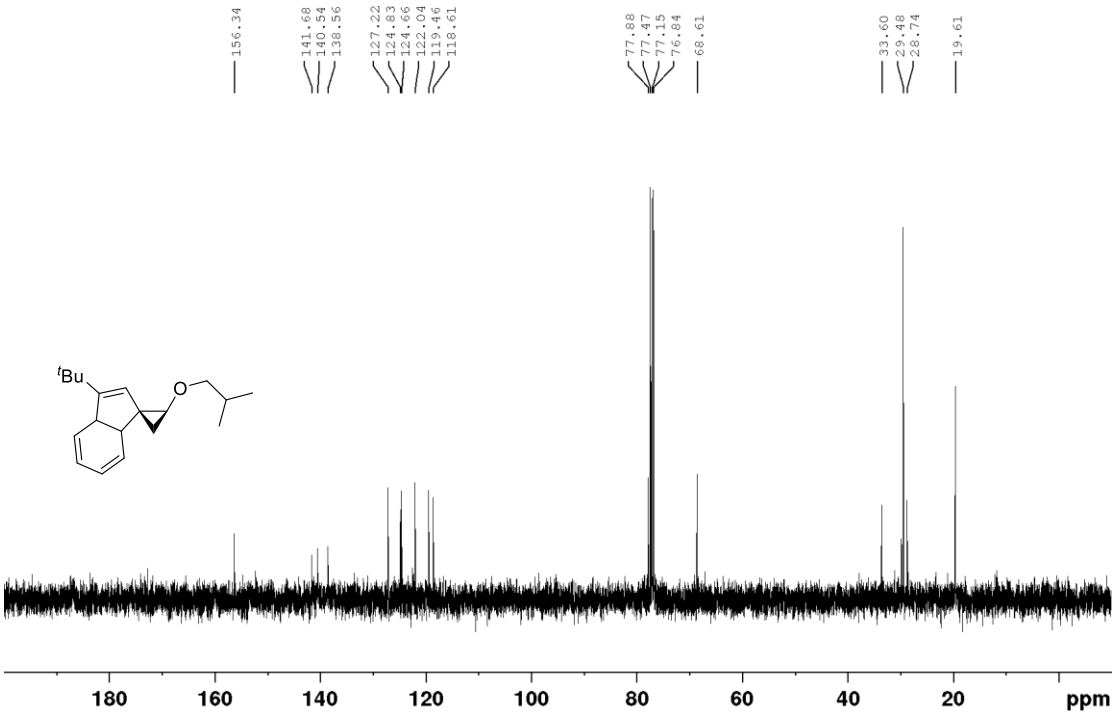

Figure S13. The ^{13}C{^{1}H} NMR spectrum of 2-*iso*-butyloxy-2'-*tert*-butylspiro[cyclopropane-1,1-indene] (**3a**) in $CDCl_3$ at 100.6 MHz.

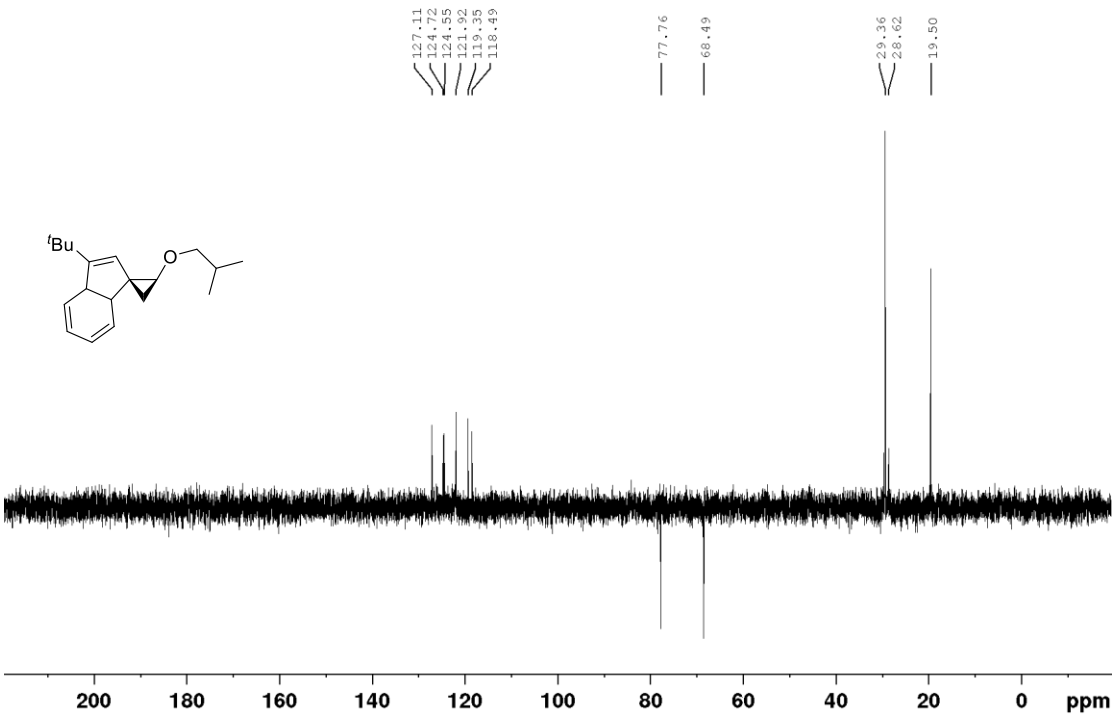

Figure S14. The DEPT135 $^{13}C\{^{1}H\}$ NMR spectrum of 2-*iso*-butyloxy-2'-*tert*-butylspiro[cyclopropane-1,1-indene] (**3a**) in $CDCl_3$ at 100.6 MHz.

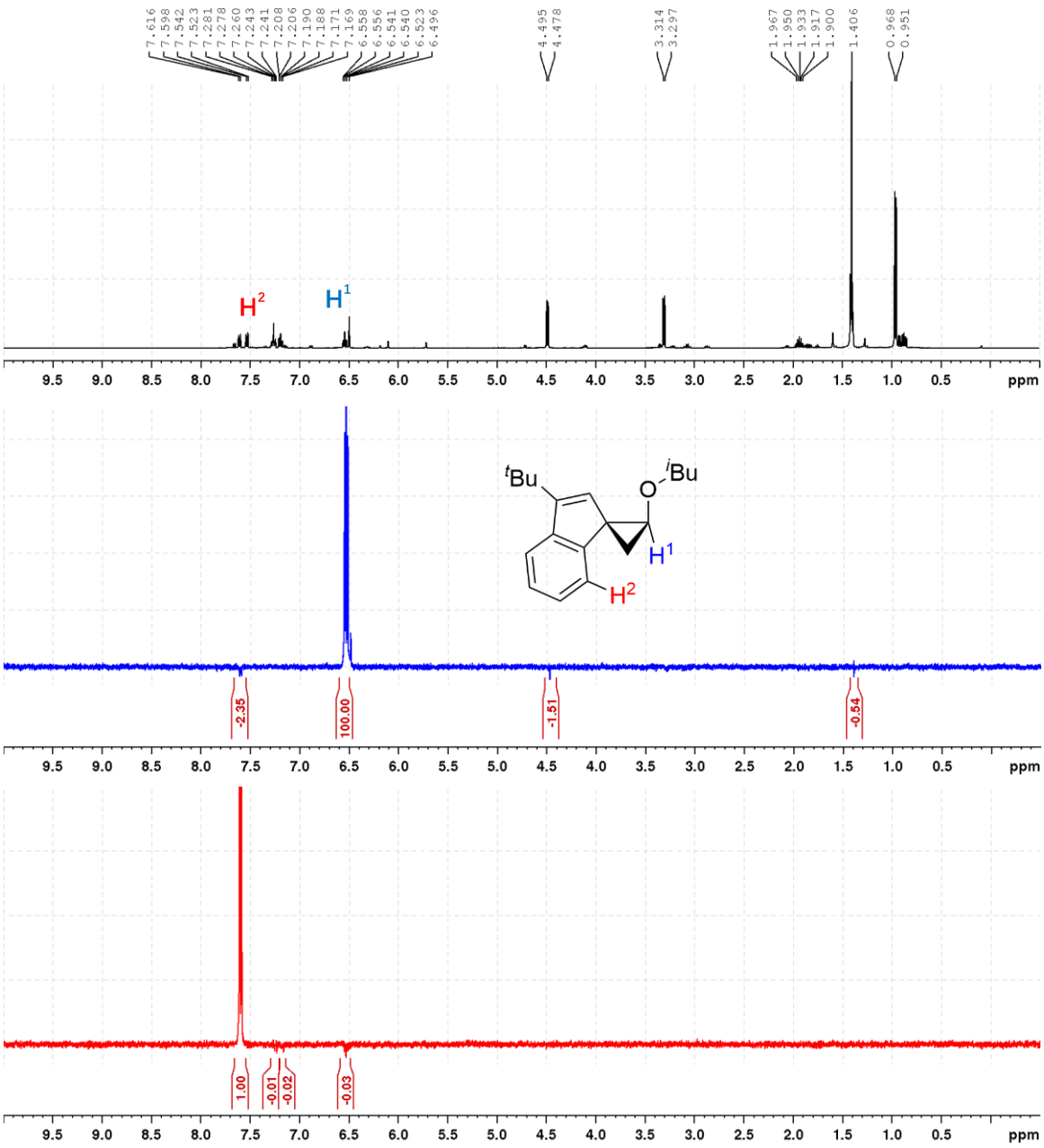

Figure S15. NOE experiments on 2-*iso*-butyloxy-2'-*tert*-butylspiro[cyclopropane-1,1-indene] (**3a**).

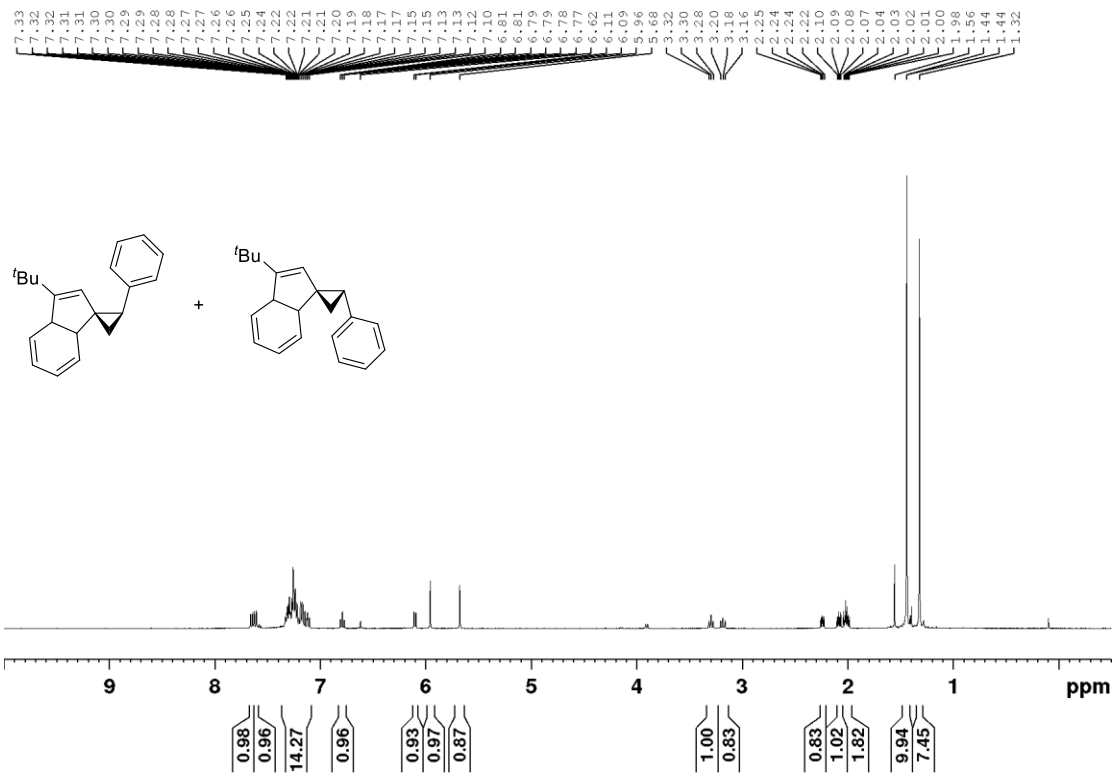

Figure S16. The ^{1}H NMR spectrum of 2-phenyl-2'-*tert*-butylspiro[cyclopropane-1,1-indene] (**3b**) in $CDCl_3$ at 400.1 MHz.

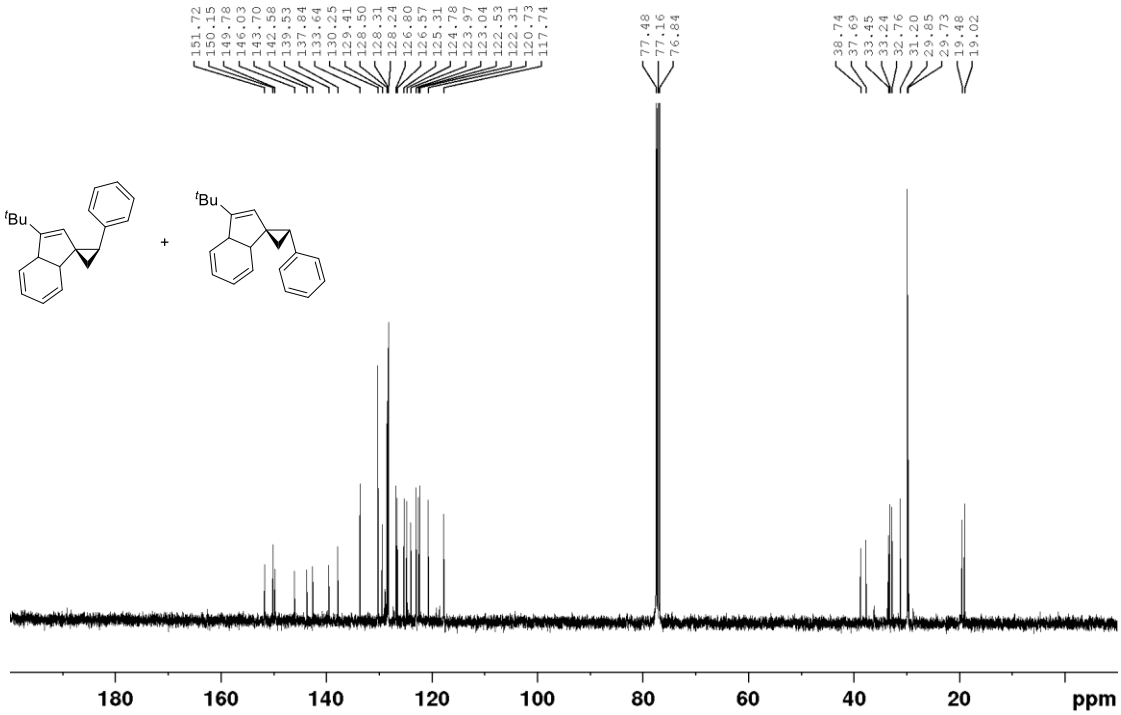

Figure S17. The $^{13}C\{^{1}H\}$ NMR spectrum of 2-phenyl-2'-*tert*-butylspiro[cyclopropane-1,1-indene] (**3b**) in $CDCl_3$ at 100.6 MHz.

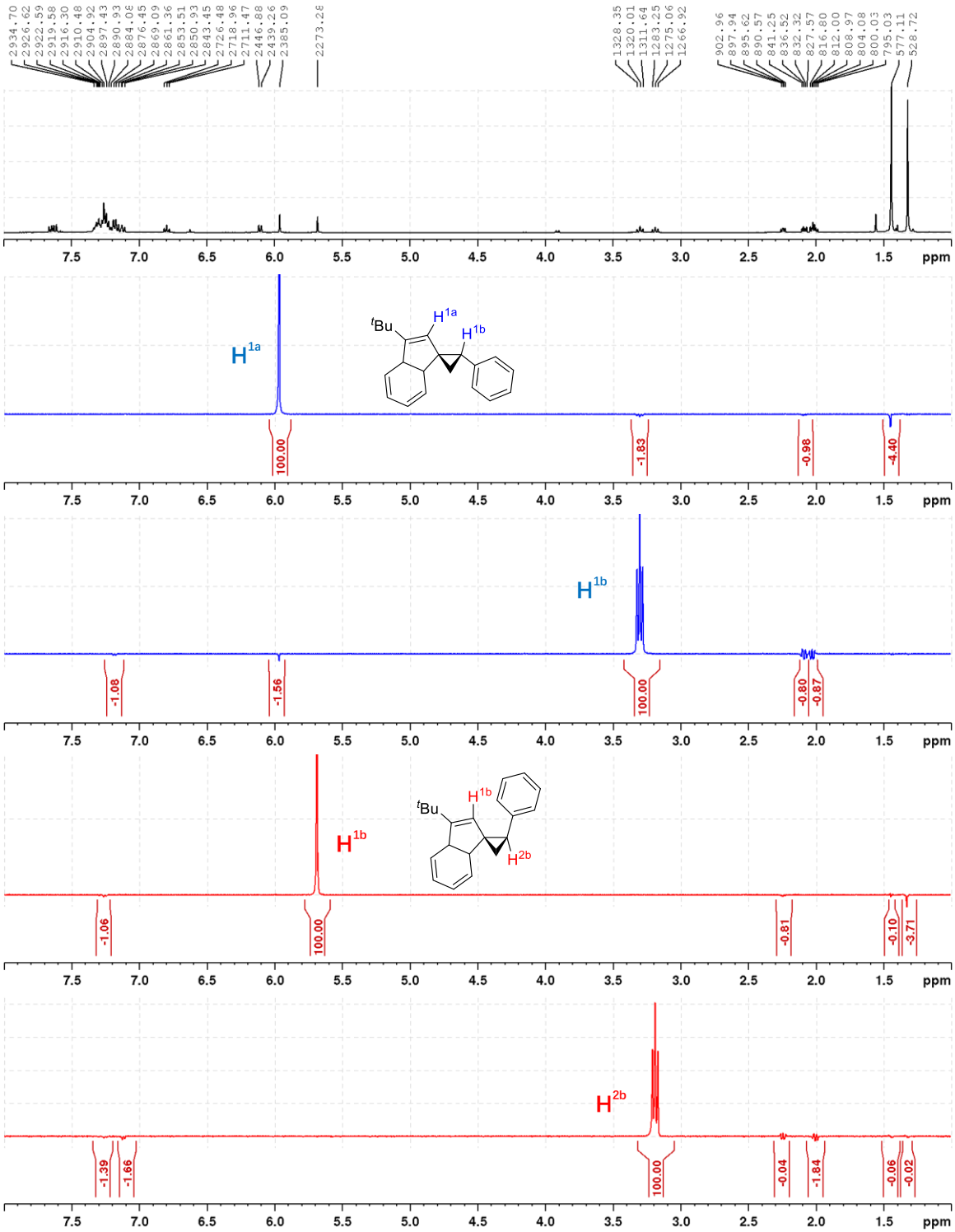

Figure S18. NOE experiments on 2-phenyl-2'-*tert*-butylspiro[cyclopropane-1,1-indene] (**3b**).